AFRL-RX-WP-TP-2008-4319

A COMPARISON OF CONTINUOUS SPD PROCESSES FOR IMPROVING THE MECHANICAL PROPERTIES OF ALUMINUM ALLOY 6111 (PREPRINT)

R. Lapovok, L.S. Tóth, M. Winkler, and S.L. Semiatin

Metals Branch
Metals, Ceramics, and NDE Division

APRIL 2008

AIR FORCE RESEARCH LABORATORY
MATERIALS AND MANUFACTURING DIRECTORATE
WRIGHT-PATTERSON AIR FORCE BASE, OH 45433-7750
AIR FORCE MATERIEL COMMAND
UNITED STATES AIR FORCE

REPORT DOCUMENTATION PAGE

Form Approved
OMB No. 0704-0188

1. REPORT DATE *(DD-MM-YY)*	2. REPORT TYPE	3. DATES COVERED *(From - To)*
April 2008	Journal Article Preprint	

4. TITLE AND SUBTITLE

A COMPARISON OF CONTINUOUS SPD PROCESSES FOR IMPROVING THE MECHANICAL PROPERTIES OF ALUMINUM ALLOY 6111 (PREPRINT)

5a. CONTRACT NUMBER
In-house

5b. GRANT NUMBER

5c. PROGRAM ELEMENT NUMBER
62102F

6. AUTHOR(S)

R. Lapovok and M. Winkler (Monash University)
L.S. Tóth (Université Paul Verlaine de Metz)
S.L. Semiatin (AFRL/RXLMP)

5d. PROJECT NUMBER
4347

5e. TASK NUMBER
RG

5f. WORK UNIT NUMBER
M02R2000

7. PERFORMING ORGANIZATION NAME(S) AND ADDRESS(ES)

Monash University

Université Paul Verlaine de Metz

Metals Branch (AFRL/RXLMP)
Metals, Ceramics, and NDE Division
Materials and Manufacturing Directorate
Wright-Patterson Air Force Base, OH 45433-7750
Air Force Materiel Command, United States Air Force

8. PERFORMING ORGANIZATION REPORT NUMBER
AFRL-RX-WP-TP-2008-4319

9. SPONSORING/MONITORING AGENCY NAME(S) AND ADDRESS(ES)

Air Force Research Laboratory
Materials and Manufacturing Directorate
Wright-Patterson Air Force Base, OH 45433-7750
Air Force Materiel Command
United States Air Force

10. SPONSORING/MONITORING AGENCY ACRONYM(S)
AFRL/RXLMP

11. SPONSORING/MONITORING AGENCY REPORT NUMBER(S)
AFRL-RX-WP-TP-2008-4319

12. DISTRIBUTION/AVAILABILITY STATEMENT
Approved for public release; distribution unlimited.

13. SUPPLEMENTARY NOTES
Journal article submitted to *Materials Science and Engineering A*. PAO Case Number: WPAFB 08-3107; Clearance Date: 29 Apr 2008. The U.S. Government is joint author of this work and has the right to use, modify, reproduce, release, perform, display, or disclose the work. Paper contains color.

14. ABSTRACT

Microstructure evolution, mechanical properties, formability, and texture development were determined for AA6111 samples processed by asymmetric rolling (ASR) with different roll friction, velocity, or diameters, conventional rolling (CR), and equal-channel-angular pressing (ECAP). highly elongated or sheared grain structures were developed during ASR/CR and ECAP, respectively. ASR led to improved r-values and formability compared to CR primarily as a result of the development of moderate shear-texture components analogous to those developed during ECAP of billet material. ASR based on different roll diameters gave the best combination of strength, ductility, and formability.

15. SUBJECT TERMS
severe plastic deformation, asymmetric rolling, equal channel angular pressing, aluminum alloy 6111

16. SECURITY CLASSIFICATION OF:			17. LIMITATION OF ABSTRACT:	18. NUMBER OF PAGES	19a. NAME OF RESPONSIBLE PERSON (Monitor)
a. REPORT	b. ABSTRACT	c. THIS PAGE			Sheldon L. Semiatin
Unclassified	Unclassified	Unclassified	SAR	36	19b. TELEPHONE NUMBER *(Include Area Code)* N/A

Standard Form 298 (Rev. 8-98)
Prescribed by ANSI Std. Z39-18

A COMPARISON OF CONTINUOUS SPD PROCESSES FOR IMPROVING THE MECHANICAL PROPERTIES OF ALUMINUM ALLOY 6111

R. Lapovok[1], L.S. Tóth[2], M. Winkler[1], and S.L. Semiatin[3]

[1]CoE Design in Light Metals, Department of Materials Engineering, Monash University, Melbourne, 3800, Australia
[2]Laboratoire de Physique et Mécanique des Matériaux, Université Paul Verlaine de Metz, Ile du Saulcy, 57045, Metz, France
[3]Air Force Research Laboratory, Materials and Manufacturing Directorate, AFRL/RXLM, Wright-Paterson Air Force Base, OH 45433-7817, USA

Abstract

Microstructure evolution, mechanical properties, formability, and texture development were determined for AA6111 samples processed by asymmetric rolling (ASR) with different roll friction, velocity, or diameters, conventional rolling (CR), and equal-channel-angular pressing (ECAP). Highly elongated or sheared grain structures were developed during ASR/CR and ECAP, respectively. ASR led to improved r-values and formability compared to CR primarily as a result of the development of moderate shear-texture components analogous to those developed during ECAP of billet material. ASR based on different roll diameters gave the best combination of strength, ductility, and formability.

Key words: Severe Plastic Deformation, Asymmetric Rolling, Equal Channel Angular Pressing, Aluminium Alloy 6111

1. INTRODUCTION

The expanding use of aluminum alloys instead of steels in automotive components is driven by the desire to reduce weight and fuel emissions. For example, the replacement of steel parts with aluminum can reduce the weight by approximately

40-50 percent [1]. However, aluminum alloys are more expensive and have inferior formability compared to steels. Among the many possible aluminum alloys for automotive applications, AA6111 in sheet form has become the most promising candidate for body panels due to its good corrosion resistance, reasonable formability, and excellent paint bake hardening to a strength level above 300 MPa without the need for a separate age-hardening step [2].

Despite significant work in the area of thermo-mechanical processing, conventional rolling techniques used to produce AA6111 sheets [3] do not yield a competitive material for auto-body applications inasmuch as the resulting formability is not sufficient to justify the manufacturing cost. Limitations in formability due to the rolling texture can be greatly reduced through the use of an additional processing step to develop a shear texture into the sheet product. For this purpose, recent attention has focussed on severe-plastic-deformation processes such as equal channel angular pressing (ECAP) which imparts large deformation in simple shear. Accordingly, a few continuous ECAP processes for sheet products have emerged [4-7], but are still under development due to problems associated with the large surface area-to-thickness ratio. Furthermore, state-of-the-art continuous ECAP equipment is not easy to implement in industrial practice because of drawbacks such as the tendency for buckling/mechanical instability and the control of sheet surface finish and thickness. In particular, recent research on continuous ECAP processing of sheet has shown that simple shear is not easy to introduce into sheet material without the superposition of bending stresses and decreases in thickness [7, 8]. Intense shear deformation (and thinning) may also lead also to temperature increases, partial recrystallization, and the formation of an undesirable cube texture.

Another well-known process which introduces simple shear through the thickness of sheet is asymmetric rolling [9-12]. Asymmetric rolling is relatively simple and overcomes a number of the shortcomings of continuous ECAP. The asymmetry of metal flow can be introduced by using different roll diameters, roll rotational speeds, or roll-surface frictional conditions. In recent work [12], it was found that subsequent sheet formability depended on the specific method used for asymmetric rolling despite the similarity in metal flow in all cases. However, a systematic study of the influence of different possessing techniques on properties and microstructure of sheet has yet to be performed.

One of the most important factors that affect formability (especially in deep-drawing operations) is crystallographic texture through its role in determining normal- and planar- plastic anisotropy (i.e., the Lankford *r*-value and Δr value, respectively). In this regard, asymmetric rolling and ECAP both give rise to beneficial textures. For example, textures developed during the asymmetric rolling of several different aluminium alloys were determined in [6, 11-13]. In [12], it was found that the *r*-value of AA1050 was significantly increased due to slight texture changes during the annealing of sheets processed under *differential-friction* conditions. Noticeable shear textures were produced with *differential-speed* rolling of AA5182 Al [13], leading to a slight increase in the *r*-value. The textures that are developed during differential-speed rolling of AA6111 have also been studied in detail in reference 11, in which it was shown that texture rotations due to shear can be modelled with a Taylor polycrystalline-plasticity model. Textures formed during the continuous ECAP of sheet have also been determined for AA1050 [6] and AA6111 [8]. Several ECAP passes were required to obtain shear textures in AA1050 sheet [6]. In both [6] and [8],

the presence of a cube (or rotated-cube) component, which is detrimental to the development of high *r*-values and good formability, was also observed.

The objective of the present work was to obtain a direct comparison of the microstructures, mechanical properties, and formability developed during both conventional and asymmetric rolling for a specific aluminum alloy, AA 6111. The resulting properties were compared to those obtained in material processed via ECAP of bulk samples as well as sheet material [8] deformed to the same level of strain. The effect of texture on the formability characteristics was also examined in detail.

2. MATERIAL AND PROCEDURES

The program material consisted of the aluminum alloy AA 61111 containing (in weight pct.) 0.74 Mg, 0.64 Si, 0.69 Cu, 0.12 Fe, and 0.17 Mn. DC-cast billets were supplied by Comalco Aluminium, Ltd. Samples with a rectangular cross-section measuring 20mm × 20mm and length of 120 mm were cut from the billet and solution treated at 500°C for 1 h followed by water quenching prior to subsequent processing. Heat-treated samples were rolled (in 18 to 25 passes) from 20-mm thickness to 2 mm (i.e., overall thickness reduction of 90 pct.) by a number of different techniques (Table 1). Other samples were subjected to one pass of ECAP at room temperature in a 90-degree die introducing an equivalent strain of 1.15 into the material. The ECAP-processed samples were then sliced in either in the y- or z- planes (Fig. 1) to obtain 2-mm thick sheets.

The microstructure of the starting and deformed materials in the plane of the sheet was characterized by optical microscopy (OM) and transmission-electron microscopy (TEM), the latter using a CM20 microscope operated at 200 kV. For this purpose, TEM foils were prepared using a twin-jet Struers Tenupol-5 electropolishing

unit and a solution of 33 pct. nitric acid in methanol at 30 V, ~200 mA, and a bath temperature of -20°C. Bright-field (BF) images and selected-area electron diffraction (SAED) patterns (with an aperture size of 1.1 μm) were taken for analysis.

The mechanical properties of material subjected to various numbers of passes were characterized via uniaxial tension testing in an Instron (Micro-Tester) 5848 machine and a small-scale Swift (flat-bottom) cup test. The tension tests were conducted at a strain rate of 0.01 s^{-1} using samples cut along the longitudinal (0º), transverse (90º), and diagonal (45°) directions. The normal plastic anisotropy (*r*-value) and planar anisotropy (Δr) were determined from the tension tests according to the procedure in ASTM Standard E 517-00. The Swift test used a 6-mm diameter punch and round disks of various diameters (between 9.5 and 14.6 mm) which had been ground and polished to the required thickness of 0.4 mm using Tenupol-1 equipment.

The plastic anisotropy and drawing behavior were interpreted in the context of the textures developed in as-deformed and deformed-and-annealed conditions. To this end, partial ($0 \leq \chi \leq 80°$) pole figures (PFs) for the (111), (200), and (220) planes were determined using in-plane samples and a GBC-MMA texture goniometer with a Cu K_α anode and a poly-capillary beam enhancer that collimates the beam to a 10×10 mm cross-section. Without imposing sample symmetry conditions, the spherical-harmonics method was used with the partial pole figures to obtain orientation distribution functions (ODFs) from which complete pole figures were obtained.

3. RESULTS AND DISCUSSION

3.1 Optical Microstructure Observations

Microstructures of the as-annealed AA6111 billet material and sheets after processing by each of the technique listed in Table 1 are shown in Fig. 2 (a-g).

The annealed material had an equiaxed structure with a grain size of 150 ± 50 μm. The microstructure of conventionally-rolled and asymmetricly-rolled sheets revealed highly-elongated grains with some evidence of non-uniformly distributed shear through the thickness for ASR_D and ASR_F (Fig. 2c, e). On the other hand, there was no clear evidence of shear for CR and ASR_V samples (Fig. 2b, d). A comparison of the microstructures in AA6111 ASR and continuous ECAP samples did not show wavy patterns of small amplitude along the RD nor non-uniform flow through the sheet thickness, two characteristics which have been observed previously [8] for continuous ECAP processing of the sheet. Superimposed bending and shear deformation was also not apparent. However, the simple-shear deformation mode during ASR was not seen clearly as for $ECAP_Y$ - processed samples (Fig. 2g). Despite the obvious shear pattern in ECAP when viewed on the y- plane, the z-plane did show large (~ 100 μm) grains and some shear bands within the grains (Fig. 2f).

3.2 TEM Microstructure Observations

High-magnification TEM images of AA6111 sheet samples after processing by each technique are shown in Fig. 3a-f; the diffraction patterns were taken at low magnification. The images revealed a very high degree of grain refinement. The grain-boundary misorientations were low for conventionally-rolled samples (Fig. 3a) and the sample processed by one ECAP pass which had been cut in z-plane (Fig. 3e). These results contrasted to the observations for the ECAP sample cut in the y-plane

(Fig. 3f) and all of the asymmetricly-rolled samples (Fig. 3b, c, d). The diffraction patterns for ASR_D and $ECAP_Y$ samples (Fig. 3b, f) were typical of those for materials which have undergone large plastic deformation, resulting in a more smeared out distribution of diffraction spots characterising increased cell misorientations.

Detailed examination of the TEM images revealed that the structure in CR samples consisted of very thick cell walls, in contrast with the other heavily deformed samples which exhibited very sharp cell walls. The ASR_D-processed samples showed the highest average dislocation density inside the cells including the formation of dislocation pile-ups and a highly tangled dislocation structure. Larger cell sizes and lower intra-cellular dislocation densities (possibly indicative of enhanced dynamic recovery and *continuous* dynamic recrystallization) were observed for samples processed by ASR_V and ASR_F (Fig. 3c, d).

3.3 Mechanical Properties

3.3.1 Tensile properties

The tensile properties of sheet samples tested along the longitudinal (0º), transverse (90º), and diagonal (45°) directions are summarized in Fig. 4-6 and Table 2.

Not surprisingly, the $ECAP_Z$ sheet exhibited tensile properties similar to those obtained after one ECAP pass and tested in bulk form [8]. Similar ductility but higher strength was obtained for ECAP sheets cut along the y-plane of the bulk ECAP sample. Moreover, sheet samples subjected to different asymmetric rolling techniques and conventional rolling demonstrated similarly high levels of strength between 218 and 256 MPa. The highest tensile ductility of ~20 pct. was obtained for ASR_D sheet. This value is far greater than the ductility measured for materials rolled by other ASR techniques and ECAP samples, i.e., < 10 pct., as well as that for conventionally-rolled sheet (12-14 pct.).

3.3.2 Plastic anisotropy

The normal plastic anisotropy or *r*-value (i.e., the ratio of the strains in the width and thickness directions of a sheet material in an uniaxial tension test) and the planar plastic anisotropy or Δr (a measure of the variation of the *r*-value with orientation within the sheet) are useful indicators of deep-drawing performance. A high r-value is advantageous as it indicates a reduced tendency to thin in the thickness direction (which typically initiates failure in a drawing operation).

The values of the *average* normal anisotropy, $\bar{r}$, and planar plastic anisotropy, Δr, are given in Table 3.

The data in Table 3 indicate that asymmetric rolling gave $\bar{r}$-values (0.64-0.82) which are slightly higher than that for conventionally-rolled material (0.62). Differential-friction rolling provided a normal anisotropy similar to that obtained via conventional rolling in agreement with previous observations [12]. Asymmetric rolling using rolls of different diameter appears to be the best ASR technique to obtain the best combination of high $\bar{r}$ and low Δr, and hence the best drawability and smallest ears during deep-drawing operations.

ECAP processing also increased $\bar{r}$ to ~0.75 which is much higher than 0.39, the value obtained for sheet processed by continuous ECAP [8]. In the previous effort, such a low value was attributed to thinning and bending stresses superimposed onto the shear deformation during ECAP of sheet. The planar plastic anisotropy was high for sheets cut in y-plane from the ECAP sample, but quite low for sheets cut in z-plane, a trend in agreement with prior results [12].

3.3.3 Deep-drawing behavior

Typical observations from the Swift cup test used to establish the effect of deformation technique on the limiting drawing ratio (LDR) are shown in Fig. 6. The $ECAP_Y$ material showed slightly larger LDR than the CR material. The maximum drawing force as a function of the ratio of disk-to-cup diameter was used to determine the LDR (Fig. 7, vertical broken lines). A comparison of the results for different processing techniques (Fig. 7, Table 4) showed that asymmetric rolling with differential friction and roll velocities gave rise to slightly lower LDR compared with conventional rolling, while asymmetric rolling with different roll diameters gave slightly higher LDR. Similar plots for ECAP-processed samples (Fig. 8, Table 4) showed noticeably greater improvement in LDR compared to asymmetric rolling, although the *r*-values after both ASR and ECAP were very similar.

3.4 Texture and Formability

3.4.1 Texture measurements

The textures after conventional rolling (CR) and different types of asymmetric rolling are displayed in Fig. 9. After CR, the texture showed the usual components including a particularly pronounced 'Cu' component (Fig. 9a). After asymmetric *friction* rolling (ASR_F), the texture was very similar to that for conventional (symmetric) rolling except that it was slightly rotated opposite to the rolling direction (by about 2°; Fig. 9b). This effect was accentuated for asymmetric rolling with a velocity differential (ASR_V) (Fig. 9c). Finally, ASR_D conditions resulted in a texture that was very different from the conventional rolling texture (Fig. 9d).

The rotations of the textures are due to a shear component of varying magnitude. With an increase in shear deformation, the texture should approach that of a shear-type texture. The shear is expected to act nearly in the rolling plane along the

rolling direction (RD). In order to estimate the effect of shear in asymmetric rolling on overall texture evolution, a {111} pole figure showing the positions of the ideal fcc shear textures in the rolling-plane projection was constructed (Fig. 10). In this figure, the shear plane is the ND plane, and the shear direction is the RD. The ideal texture components shown in the pole figure are summarized in Table 5. The two ideal shear fiber textures are also identified in Fig. 10: the A fibre (with its A, A1, and A2 components) and the B fiber (along which there are the A, B and C orientations). Note that there is a distinction between A and $\overline{A}$ as well as between the B and $\overline{B}$ components in Table 5; both of them are called simply the A component in Fig. 10 for the reason that they are expected to have the same intensities, respectively, due to the two-fold symmetry around the RD in asymmetric rolling.

It is well known that a <111> || ND improves formability while <001> || ND reduces it [14]. As can be seen in Fig. 10, the A fiber of simple shear is actually a <111> || ND fiber if shear is taking palace within the ND plane. Thus, this texture component improves formability. However, the C orientation, which is usually of high intensity in the textures of aluminum [15], is a (001)[110] orientation that leads to reduced formability.

A comparison of the textures developed during asymmetric rolling and the ideal orientations due to simple shear indicates that the rolling textures were far from the ideal shear textures. The ASR_D texture deviated most from the symmetrical-rolling case. The identification of the ideal components of the ASR_D texture in terms of ideal shear textures is discussed further below.

The texture after one-pass ECAP is shown in Fig. 11 in both the ND and TD views. Using the ND view, the ECAP texture was found to be very different from the rolling textures (Fig. 9). The reason for this behaviour is that the ECAP texture is 100

pct. shear in which the shear plane lies at 45° with respect to ND. The <111> || ND component of this texture was very pronounced for the ECAP case because of the strong intensity of the texture near the center of the pole figure. The <111> || ND fiber (indicated by the broken circle in Fig. 11a), however, is only a partial one.

Typically, shear textures are studied more conveniently from the TD direction, not from the ND. This is why the TD-view pole figure is shown in Fig. 11b. With the help of the key ideal ECAP orientations (Fig. 12), the texture can be characterized by a strong C component with lower intensity A and A1 components.

For a better understanding of the relation between shear and rolling textures, the rolling textures are also shown in the TD view in Fig. 13. The ideal components of the shear texture are also plotted in the same projection (Fig. 14). Detailed inspection of the location and the intensity of the rolling-texture components in conjunction with the ideal components of the shear texture (Fig. 14) revealed that there are large differences for all cases. For example, the reflections of the C shear components were not all found (Fig. 13) indicating that C was not an ideal component for rolling. There was also a continuous fibre between the A-$\bar{A}$ locations in rolling while it is not an ideal region in shear. The only certain sign of the presence of shear in the asymmetricly rolled textures was a *tilt* of the texture from its symmetrical position. This rotation was the largest for the ASR_V case. Such rotations are well known in shear and caused by the asymmetric nature of the lattice rotation field [16].

The texture corresponding to ASR_D processing had a character distinct from the other ASR processes. Specifically, it seemed to be similar to the texture that can be obtained in ECAP. This can be seen by comparing this texture with the ideal texture positions of ECAP presented in Fig. 12. The similarity is striking, although there is a ~10° rotation difference between them. In this way, the texture obtained via

ASR_D can be identified with a strong A component together with a weaker A2 component. A and A2 are actually present in all textures, although in a 10-15° rotated position. These components, however, correspond to a shear that is far from the rolling plane.

3.4.2 Relation between texture and formability

The texture characteristics presented in the preceding section can now be used in the interpretation of the formability of material processed via ASR or ECAP.

The ASR_D case contrasted with the other two asymmetric rolling methods with respect to the texture that was developed and the resulting mechanical properties. First, the tensile yield strength after ASR_D (Table 2) was the lowest among all the results for ASR and conventionally-rolled materials. This can be rationalized on the basis of the A texture component that lay at ~45° with respect to the sheet normal. This implies that there were many crystals with their {111} planes oriented near 45° to the RD direction. During tension testing, these planes would have been in a favourable position for slip because they coincided with the maximum shear stress plane. Therefore, single slip of systems with a high Schmid factor was favored. Moreover, the positions of the other three {111} slip planes were such that they would have enabled single slip during tension tests for samples lying either 45° or 90° to the RD. For these latter tests, however, the geometrical situation was less ideal than for the RD tension test.

The measured *r*-values (Table 3) for all processing methods, except $ECAP_z$, were generally smaller for RD tension tests. The interpretation of this observation again can be related to the A texture component present in all cases to varying degrees and with various tilts. The deformation related to this component when pulling the sample in the RD direction is of key interest. Considering the ideal position of A,

single slip is favoured for one of the {111} planes of A-oriented crystals that are oriented at 45° with respect to RD and also at 45° with respect to ND. At the same time, the slip direction is perpendicular to TD. For this ideal case, there would be no change in the width of the specimen. Thus, the r value would be zero. In reality, A was not the only texture component; there were other components which gave rise to higher r values. Nevertheless, a strong A component did indeed lead to the low RD r values shown in Table 3.

The ductility of the ASR_D-processed material was outstanding with respect to that from all other processes, including even ECAP (Table 2, Fig. 5). Again, this behavior can be related to the shear nature of the deformation during tension of ASR_D and possibly lower rates of cavity nucleation or growth that control ductility. The deep drawability of the ASR_D material is also marginally better than that produced by other techniques, an effect attributable to its higher value of $\bar{r}$. For these reasons, ASR_D is the most promising of the asymmetric-rolling techniques with respect to improving sheet-metal formability.

The ECAP-processed material also exhibited interesting formability characteristics, particularly its deep-drawing capacity, which is the highest among all of the processes. This benefit can be attributed to its strong <111> || ND fiber (Fig. 11a). From an analysis of the ideal orientations in ECAP textures (Fig. 12), one can speculate on the best possible <111> || ND fiber that would provide the best drawing capacity. It is apparent from Fig. 12 that a counter-clockwise rotation of ~10° would result in close coincidence of the {111} reflections of the C component with the <111> || ND fiber. To obtain such a texture, it can be shown that a die angle of ~110° is required.

When larger ECAP die angles are used, several passes are necessary to obtain textures that would lead to improved formability [6]. The process known as 'frictional angular extrusion', in which material is fed into the ECAP die with the help of friction, falls into this category. Such processes, however, can give rise to temperature increases accompanying the large plastic strain resulting in the formation of a cube or rotated cube texture component due to recrystallization. Such a component leads to poor formability. A nearly pure cube component has been obtained using a similar continuous ECAP-sheet process [8].

Conclusions

The ECAP of bulk AA6111 produces material with relatively good mechanical properties, a shear texture, and hence high *r*-values. On the other hand, continuous ECAP of sheet produces inferior LDR and *r*-values [8]. The reason of this deterioration appears to be the formation of a cube texture due to deformation heating induced by high per-pass strain and high friction heating at the surfaces of the sheet, hence leading to recrystallization. Because of the much smaller per-pass strains imposed during asymmetric rolling (ASR), such an effect is minimized for sheet materials, resulting in improved mechanical properties. It has been found that all three variants of ASR (comprising differential roll friction (F), speed (V), or diameter (D)) introduce shear deformation and improved *r*-values and LDRs for AA6111 sheet. The improvement is greatest for ASR_D and least for ASR_F. ASR_D produces high tensile ductility, comparatively higher average normal anisotropy ($\bar{r}$), low planar anisotropy (Δr), and a simple-shear texture significantly different from that developed during conventional rolling but similar to that produced by ECAP.

Acknowledgements

The authors gratefully acknowledge the support provided by the Air Force Office of Scientific Research and its Asian Office of Aerospace Research and Development (Drs. Ken Goretta, J.P. Singh, and J.S. Tiley, program managers). The authors would also like to express their gratitude to Professors Warren Poole from the University of British Columbia (Canada) and Yuri Zilberg from National Metallurgical Academy of Ukraine (Ukraine) for help with asymmetric rolling experiments.

References

[1] S.A. Mariano, F.R Tuler, and W.S. Owen, "Comparing Steel and Aluminum Auto Structures by Technical Cost Modeling," *JOM*, 6 (1993), 20-22.

[2] D.J. Lewis and Associates Pty Ltd., *Aluminium: Growth Opportunities in the Automotive Industry*, (Australia: Department of Industry, Science and Technology, 1995), p. 20.

[3] R. Lapovok, J. Y. Yao, and S. Ringer: *On the Application of 6xxx Al Alloys in Automotive Body Sheet Applications*, in *CAST Report 2001137*. 2001, Cooperative Research Centre for Cast Metals Manufacturing.

[4] A.A. Zisman, V.V. Rybin, S.Van Boxel, M. Seefeldt, B. Verlinden, "ECAD of Aluminium Sheet," *Mater. Sci. Eng. A*, A427 (2006), 123-129.

[5] Y.H. Jin, M.Y. Huh, and Y.H. Chung, “Evolution of Textures and Microstructures in IF-Steel Sheets during Continuous Confined Strip Shearing and Subsequent Recrystallization Annealing, *J. Mater. Sci.*, 39 (2004), 5311-5314.

[6] Y. Huang and P.B. Pragnell, “Continuous Frictional Angular Extrusion and Its Application in the Production of Ultrafine-Grained Metals,” *Scripta Mater.*, 56 (2007), 333-336.

[7] R. Lapovok, P.W.J. McKenzie, P.F. Thomson, and S.L. Semiatin,, “Processing and Properties of Ultrafine-Grain Aluminum Alloy 5005 Sheet, **,** *J. Mater. Sci.*, 45 (2007), 1649-1659.

[8] R. Lapovok, I. Timokhina, P.W.J. McKenzie, and R. O’Donnell, “Processing and Properties of Ultrafine-Grain Aluminum Alloy 6111 Sheet,” *J. Mater. Proc Techn.,* 200 : 1-3, (2008), pp. 441-450

[9] J.K. Kim, Y.K. Jee, M.Y. Huh, H.-T. Jeong, “Formation of Texture and Microstructure in Asymmetricly Cold Rolled and Subsequently Annealed Aluminum alloy 1100 Sheets,” *J. Mater. Sci.*, 39 (2004), 5365-5369.

[10] G.Y. Tzou, “Relationship between Frictional Coefficient and Frictional Factor in Asymmetric Sheet Rolling,” *J. Mater. Proc Techn.*, 86 (1999), 271-277.

[11] H. Jin and D.J. Lloyd, “Evolution of Texture in AA6111 Aluminum Alloy after Asymmetric Rolling with Various Velocity Ratios between Top and Bottom Rolls,” *Mater. Sci. Eng. A*, A465 (2007), 267-273.

[12] H. Utsunomiya, T. Ueno, and T. Sakai, “Improvement in the r-Value of Aluminum Sheets by Differential-Friction Rolling,” *Scripta Mater.*, 57 (2007), 1109-1112.

[13] T. Sakai, K. Yoneda, and S. Osugi, “Microstructure and Texture Control of Al-Mg Alloy Sheets by Differential Speed Rolling, *Mat. Sci. Forum*, 495-497 (2005), 507-602.

[14] M. Hatherly, W.B. Hutchinson: *An Introduction to Textures in Metals*, Institution of Metallurgists, London, 1979.

[15] F. Montheillet, M. Cohen, and J.J. Jonas, “Axial Stresses and Texture Development During the Torsion Testing of Al, Cu and alpha -Fe” *Acta Metall.*, 32 (1984) 2077-2089.

[16] L.S. Tóth, P. Gilormini, and J.J. Jonas, “Effect of Rate Sensitivity on the Stability of Torsion Textures,” *Acta Metall.*, 36 (1988), 3077-3091.

[17] P.H Lequeu and J.J. Jonas, “ Modelling of The Plastic Anisotropy of Textured Sheet,” *Metall. Trans., A*, 19A (1988), 105-120.

Table 1. Different techniques used to process AA6111 sheet

Designation	**Technique**	**Comments**
CR	Conventional Rolling	No lubricant, diameter of both rolls: 90 mm
ASR_V	Asymmetric Rolling	Differential velocity with angular speed ratio: $\omega_1/\omega_2 = 2$
ASR_D	Asymmetric Rolling	Differential roll diameters with ratio: $d_1/d_2 = 2$
ASR_F	Asymmetric Rolling	Differential friction, one sheet surface dry; the other lubricated with mineral oil
$ECAP_Y$	1 pass ECAP	Bulk sample sliced into sheets in y - plane
$ECAP_Z$	1 pass ECAP	Bulk sample sliced into sheets in z - plane

Table 2. Yield strength, tensile strength, and tensile ductility for AA6111 sheet processed by various techniques.

Test Direction	CR	ASR_V	ASR_D	ASR_F	$ECAP_Z$	$ECAP_Y$
	Yield Strength, σ_y (MPa)					
0º	203	225	167	227	154	199
90º	199	203	156	224	165	205
45º	202	210	170	221	175	200
	Ultimate Tensile Strength, σ_u (MPa)					
0º	255	246	223	242	165	211
90º	256	215	218	245	181	225
45º	247	233	234	235	196	214
	Total Elongation (pct.)					
0º	13	8.3	17.8	9.3	9.2	8.5
90º	12	6.4	20.2	8.8	7.1	7.9
45º	14	5.5	20.0	9.4	6.5	7.3

Table 3. Normal and planar plastic anisotropy measurements*

Processing Condition	r_0	r_{90}	r_{45}	$\bar{r}$	Δr
CR	0.45	0.92	0.56	0.62	0.13
ASR_V	0.61	0.69	0.81	0.73	0.16
ASR_D	0.77	0.94	0.79	0.82	0.06
ASR_F	0.55	0.85	0.86	0.64	0.16
$ECAP_Z$	0.75	0.73	0.67	0.71	0.07
$ECAP_Y$	0.55	0.72	0.99	0.81	0.36

* $\bar{r} = (r_0 + 2r_{45} + r_{90})/4$; $\Delta r = (r_0 - 2r_{45} + r_{90})/2$

Table 4. LDR (maximum disk diameter : punch diameter) measurements

Process:	CR	ASR_V	ASR_D	ASR_F	$ECAP_Z$	$ECAP_Y$
LDR:	1.77	1.74	1.80	1.72	1.96	1.94

TABLE 5. Ideal texture components for deformation via simple shear [16].

Component designation	**Miller indices (shear plane) [shear direction]**
A	$(11\bar{1})\,[1\bar{1}0]$
$\overline{\text{A}}$	$(\bar{1}\,\bar{1}\,1)\,[\bar{1}10]$
B	$(11\bar{2})\,[1\bar{1}0]$
$\overline{\text{B}}$	$(\bar{1}\,\bar{1}\,2)\,[\bar{1}10]$
C	$(100)\,[0\bar{1}1]$
A_1^*	$(11\bar{1})\,[2\bar{1}1]$
A_2^*	$(1\bar{1}1)\,[\bar{2}\bar{1}1]$
{111} fibre	$\{111\} < u\ v\ w >$
<111> fibre	$\{h\ k\ l\} < 110 >$

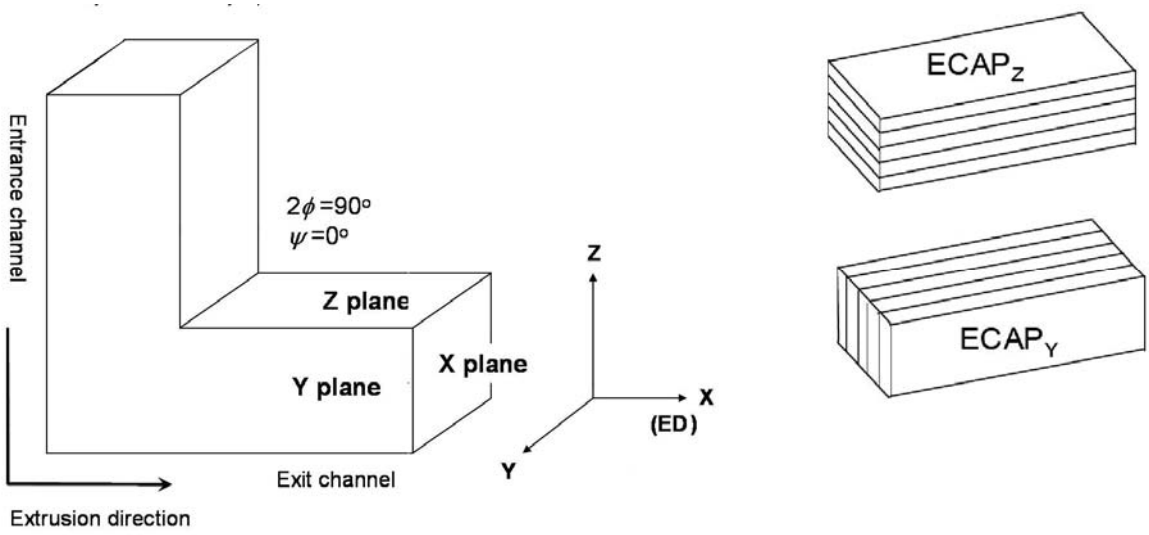

Fig. 1. Schematic illustration of the method used to cut sheet from bulk ECAP samples.

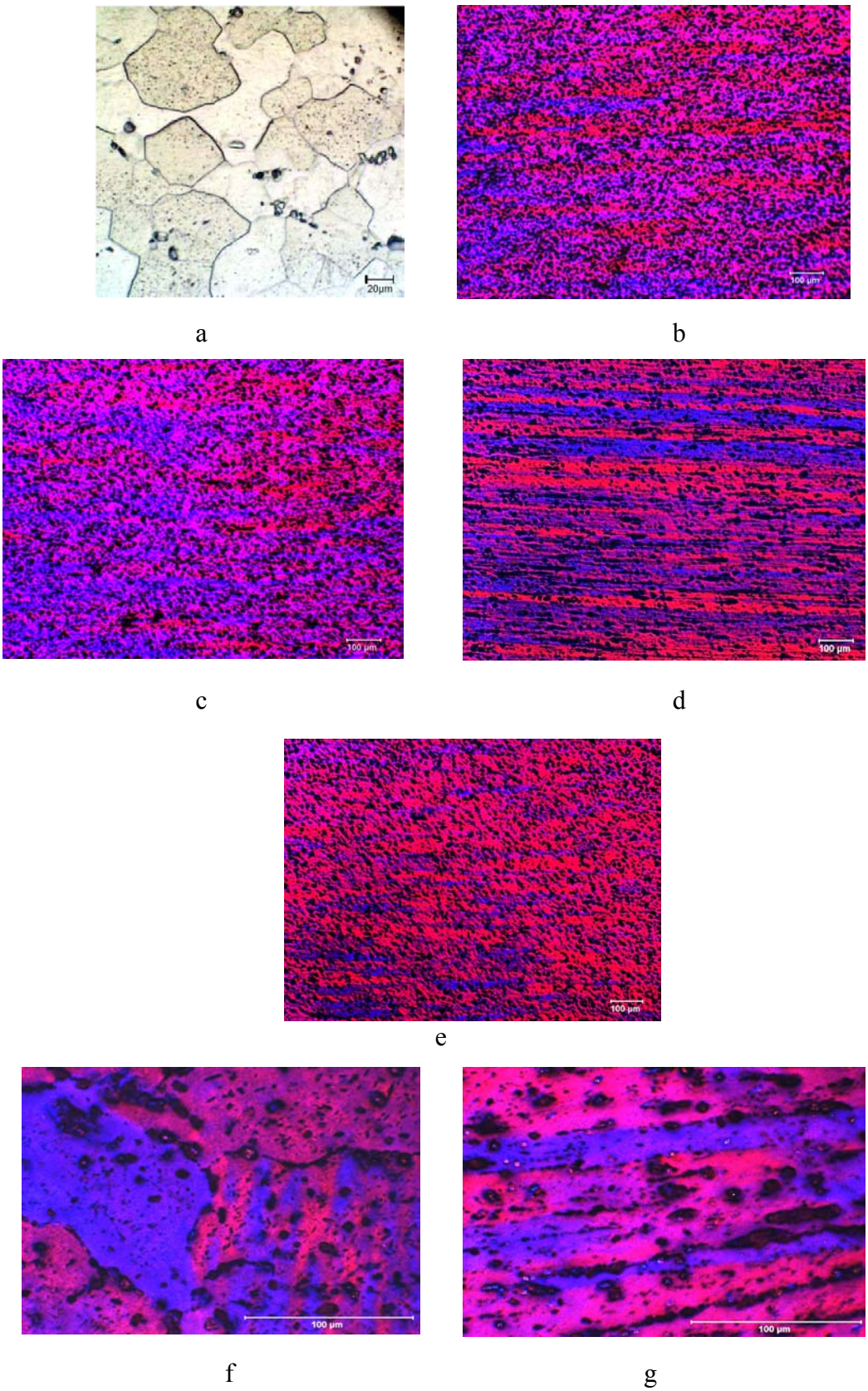

Fig. 2. Optical micrographs of AA6111 (in thickness cross-section):
(a) Billet annealed at 500^{o}C for 1h, and sheet samples following processing via (b) CR, (c) ASR_D, (d) ASR_V, (e) ASR_F, (f) $ECAP_Z$, (g) $ECAP_Y$

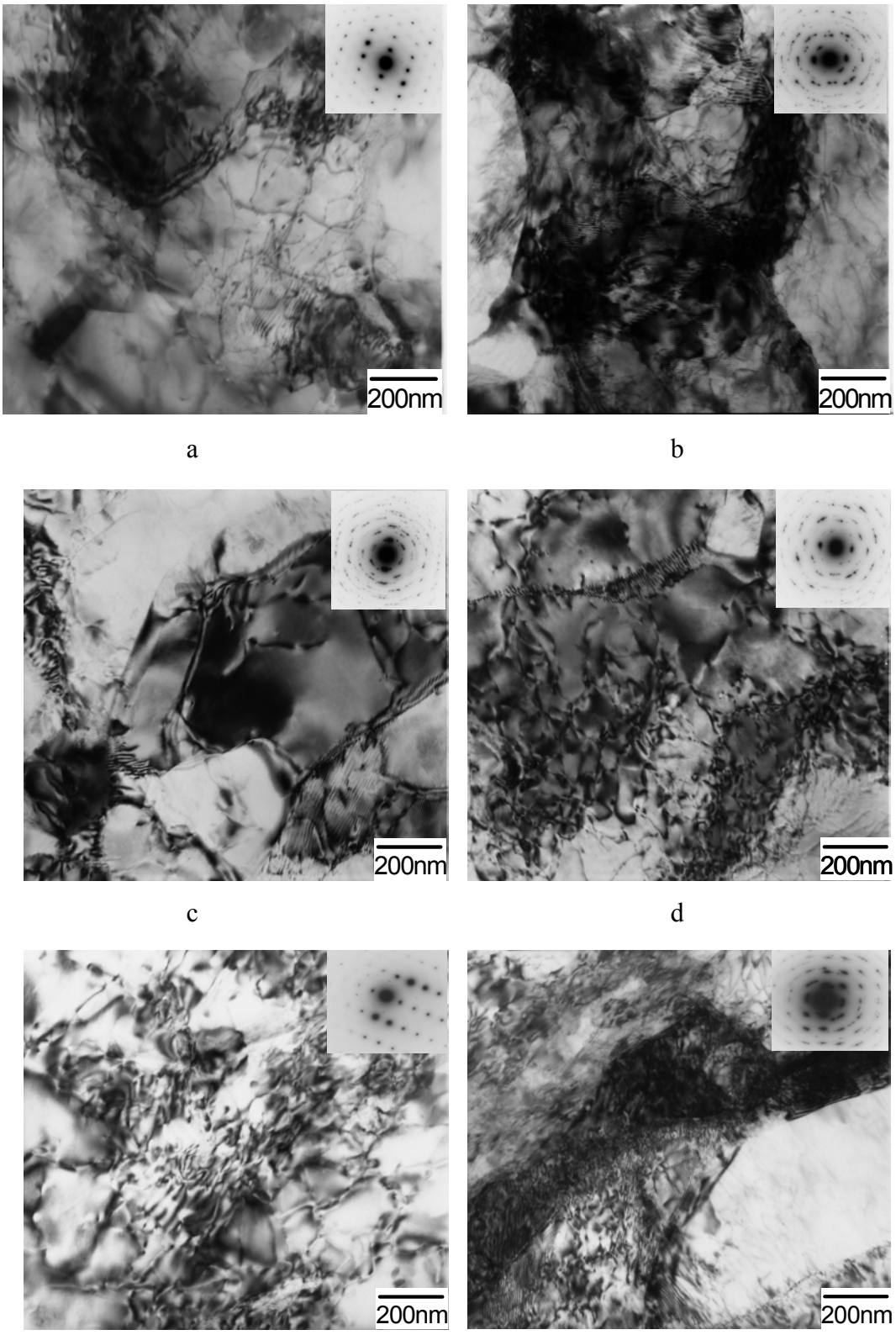

Fig. 3. TEM images of AA6111 sheet samples processed by different techniques: (a) CR, TD plane, (b) ASR_D , TD plane, (c) ASR_V , RD plane, (d) ASR_F , RD plane, (e) $ECAP_Z$, and (f) $ECAP_Y$

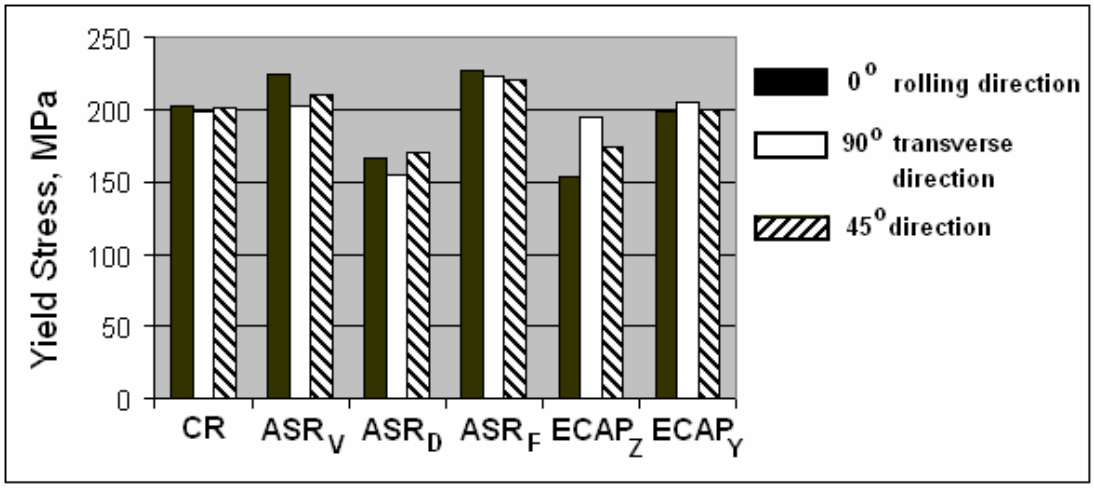

Fig. 4. Yield strength as a function of processing technique for samples cut along the rolling, transverse, and 45º directions.

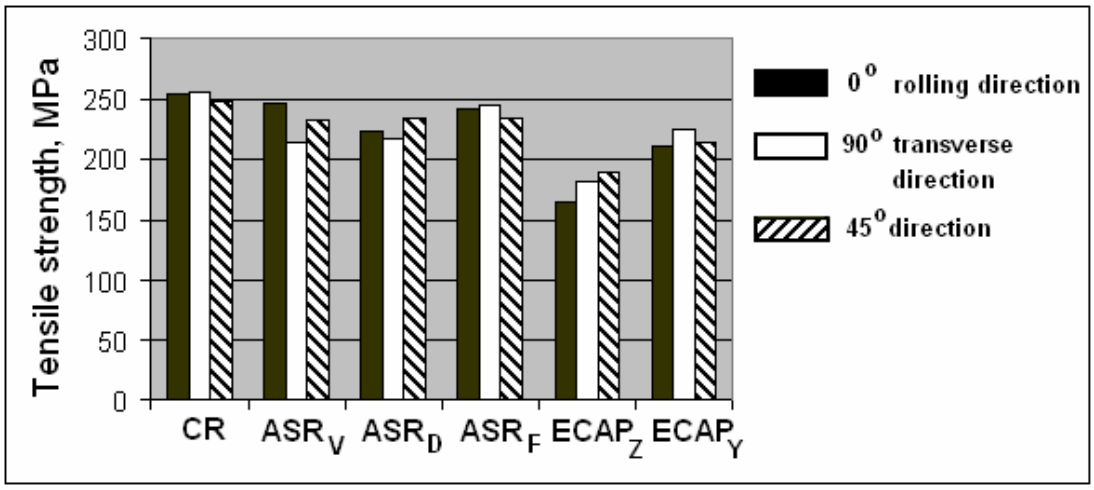

Fig. 5. Tensile strength as a function of processing technique for samples cut along the rolling, transverse, and 45º directions.

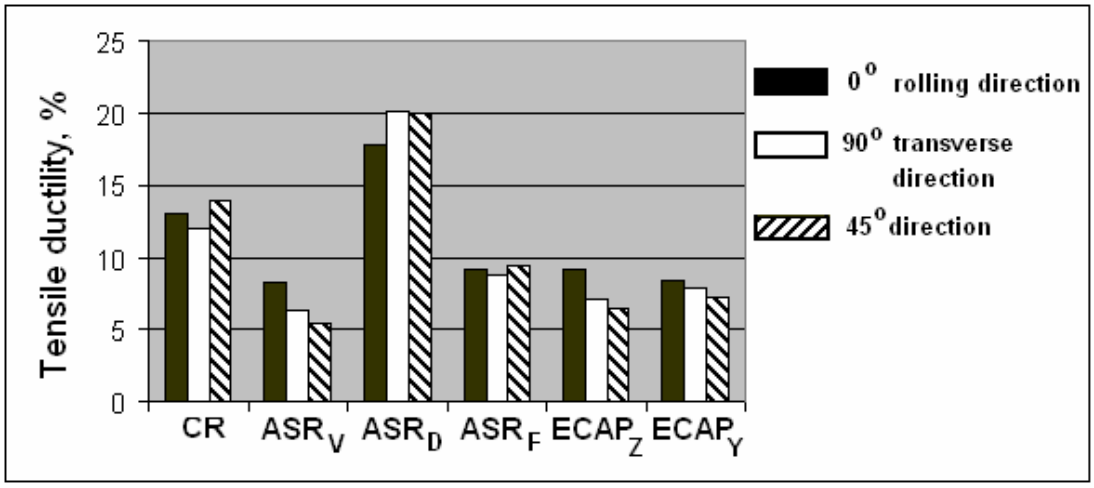

Fig. 6. Tensile ductility as a function of processing technique for samples cut along the rolling, transverse, and 45º directions.

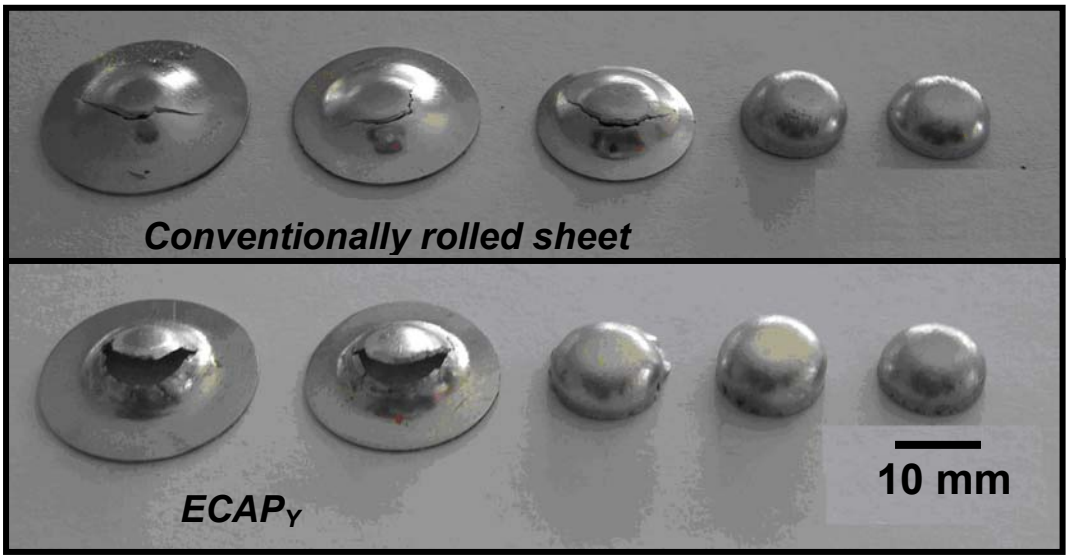

Fig. 6. Typical observations from the Swift deep-drawing test.

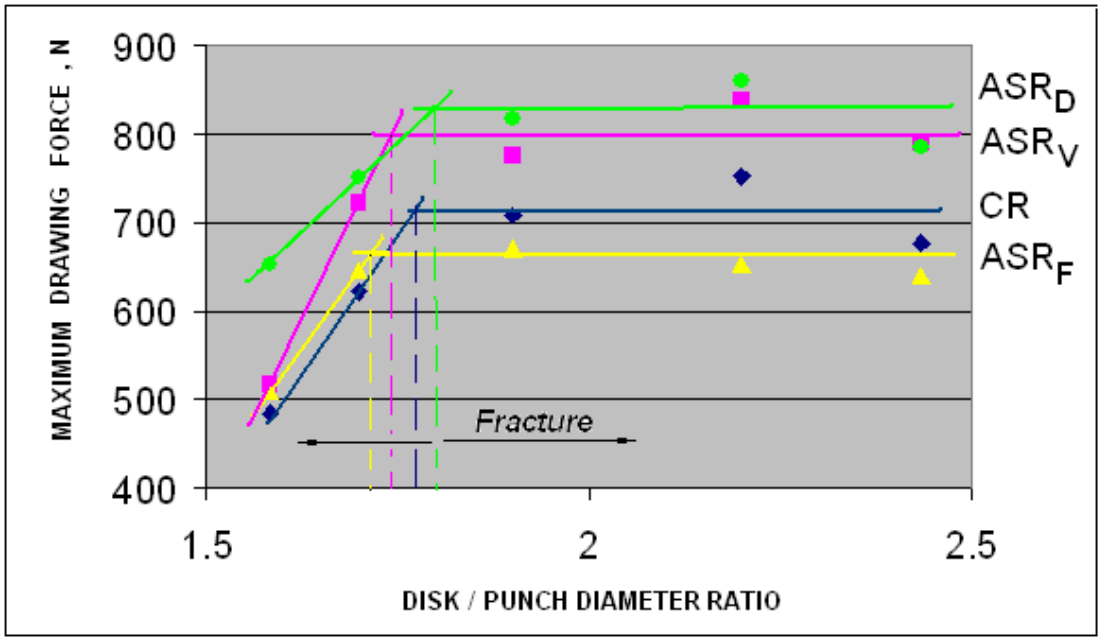

Fig. 7. Swift-test results for AA6111 sheet samples processed via conventional rolling and different asymmetric-rolling techniques.

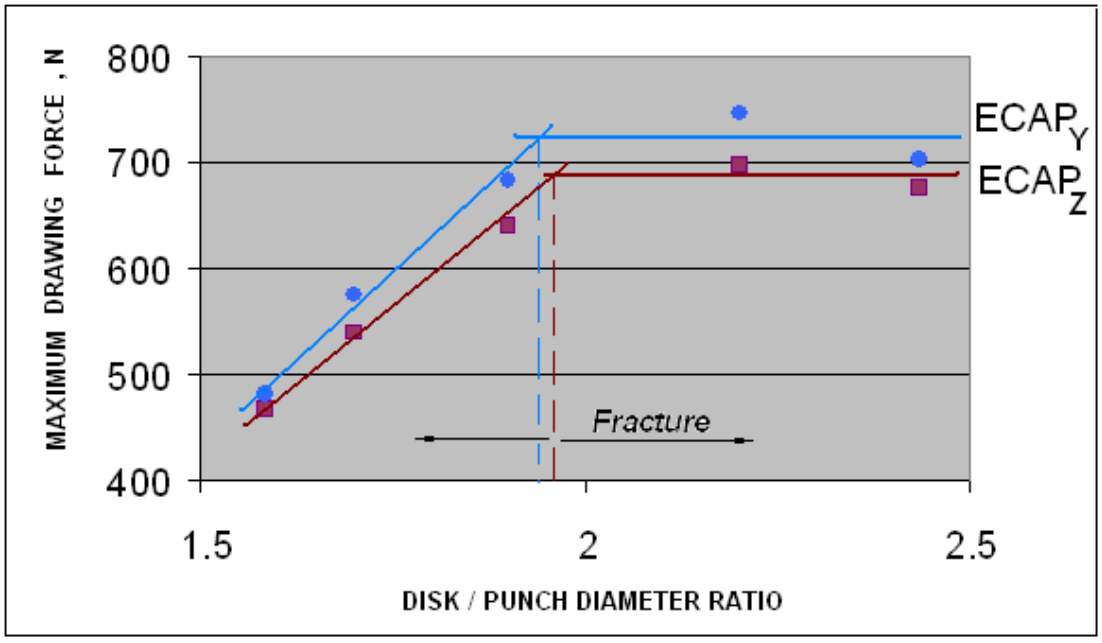

Fig. 8. Swift test results for AA6111 sheet samples extracted from the z- and y-planes of material processed via one-pass ECAP.

.

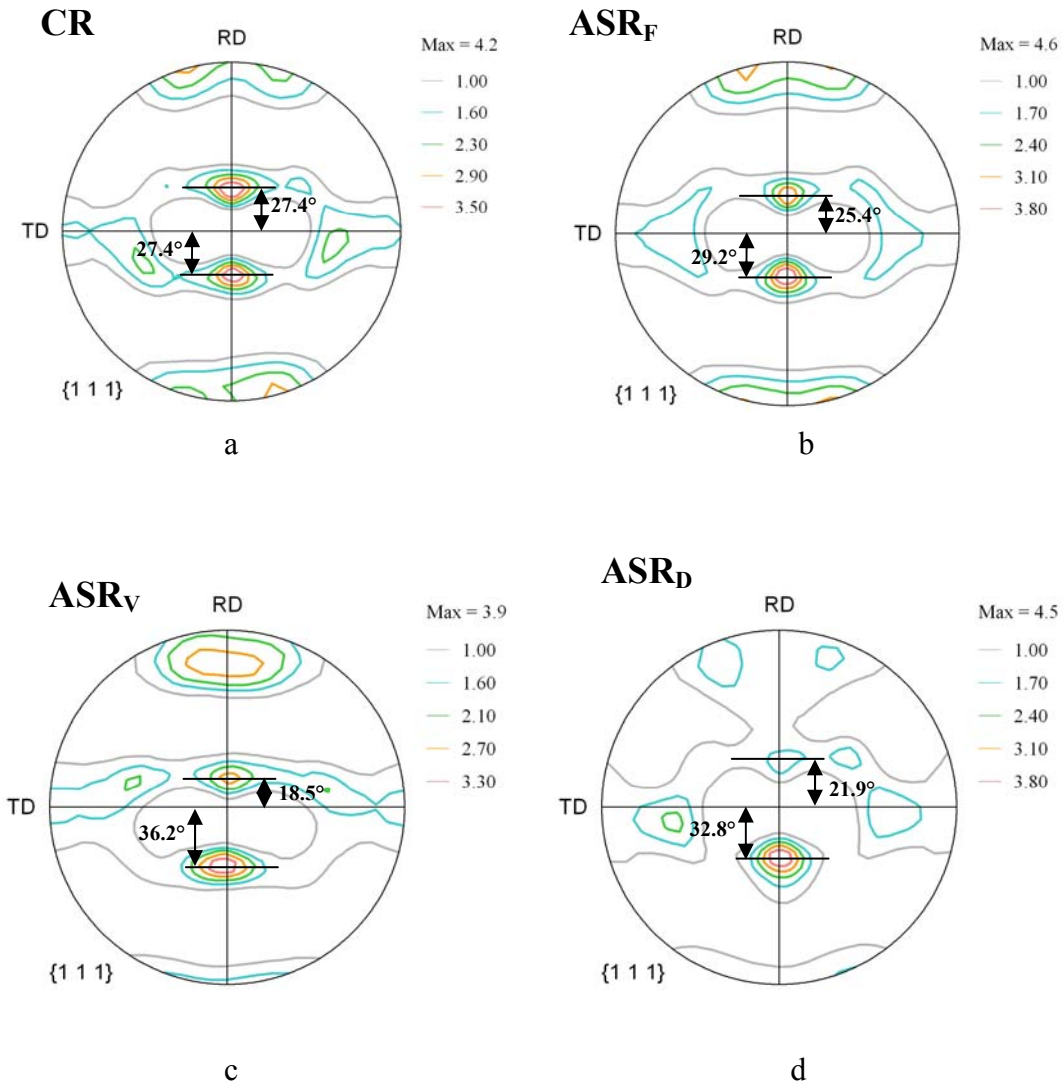

Fig. 9. Textures (in terms of {111} pole figures) developed in AA6111 sheet during different types of rolling: (a) Conventional (symmetrical) rolling, (b) asymmetric rolling with different friction conditions, (c) asymmetric rolling with differential roll velocities, and (d) asymmetric rolling with differential roll diameters.

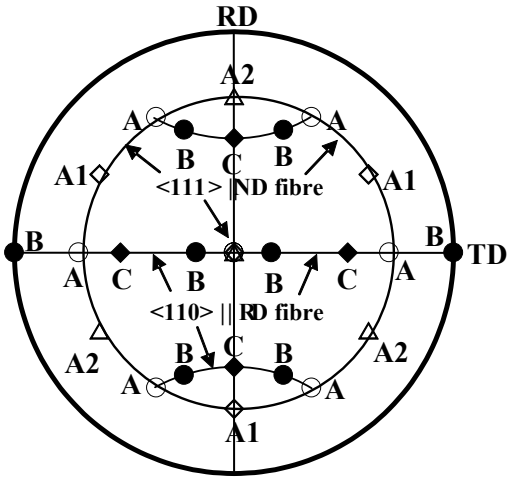

Fig. 10. Ideal orientations of fcc shear textures projected onto the ND plane. The shear plane is the ND plane; the shear displacement is in the RD direction.

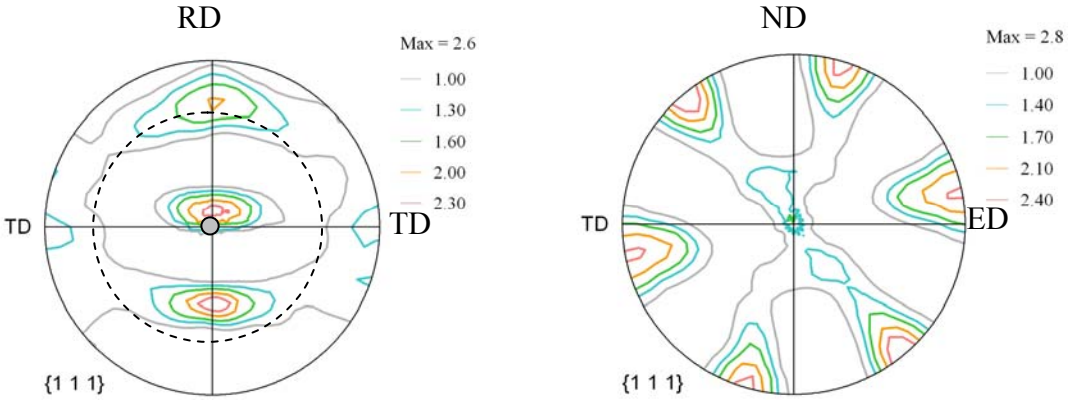

Fig 11. The texture measured after one-pass ECAP (using a 90° die) of AA6111 from both the (a) ND and (b) TD views. The broken circle and the central point indicate the position of the ideal <111> || ND fiber in (a).

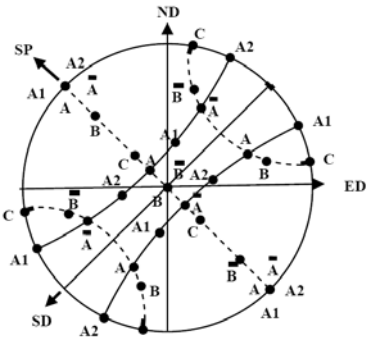

Fig. 12. The ideal positions of shear components in a (111) pole figure on the TD projection for ECAP with a 90° die. SP indicates the shear plane, and SD is the shear direction (parallel to the plane of intersection of the two channels).

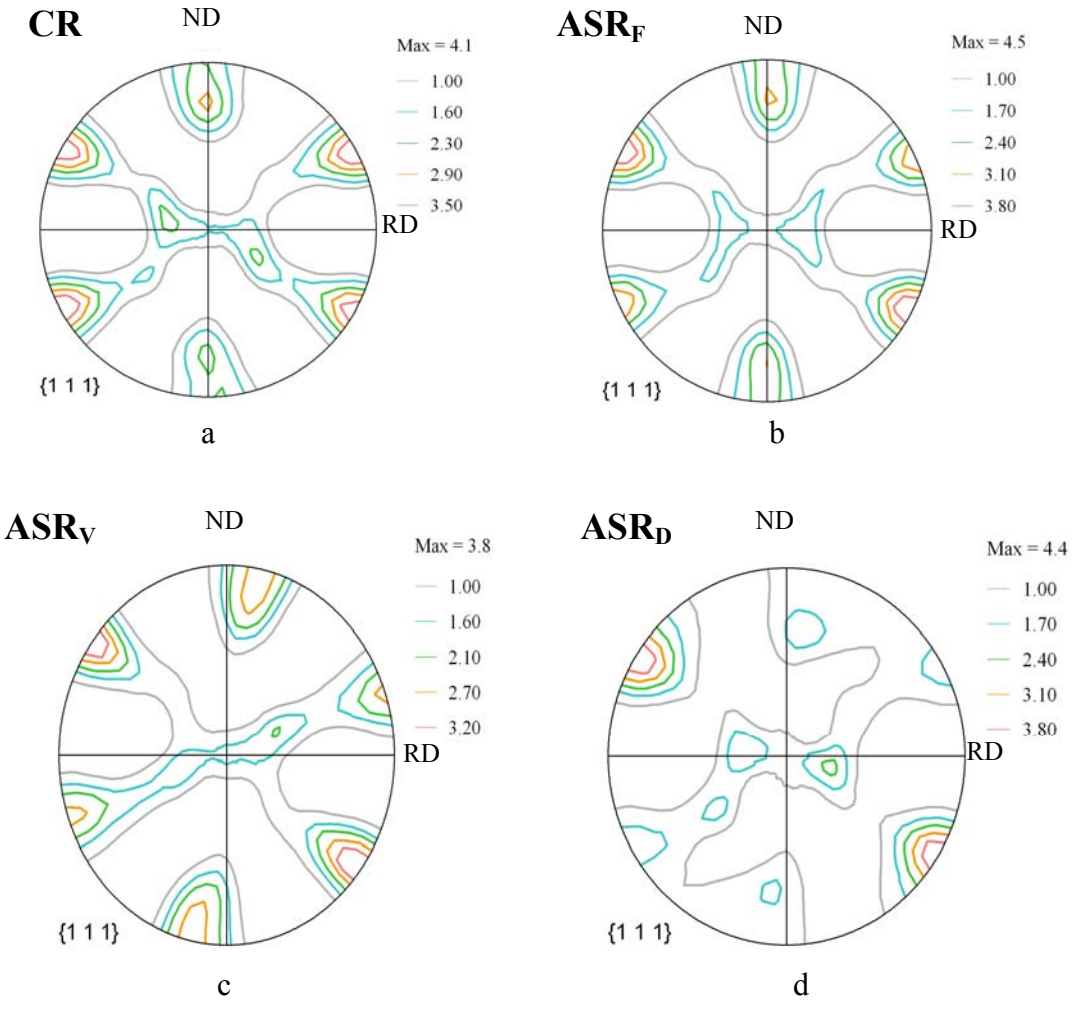

Fig. 13. Textures (in terms of (111) pole figures on the TD projection) developed in AA6111 via:
(a) Conventional (symmetrical) rolling, (b) asymmetric rolling with different friction conditions, (c) asymmetric rolling with differential roll velocities, and (d) asymmetric rolling with differential roll diameters.

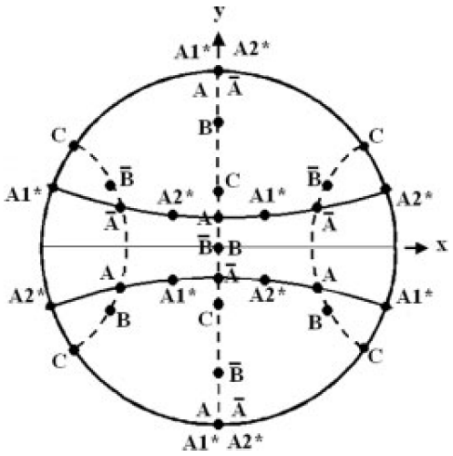

Fig. 14. Ideal orientations for shear textures in a TD projection.